Infrared spectroscopy of N₂ adsorption on size selected cobalt cluster cations in isolation

Sebastian Dillinger, Jennifer Mohrbach, Joachim Hewer, Maximilian Gaffga and Gereon Niedner-Schatteburg

We report IR active N₂ stretching frequencies in isolated and size selected cobalt cluster nitrogen adsorbate complexes, $[Co_n(N_2)_1]^+$ as recorded by virtue of InfraRed Photon Dissociation (IRPD) spectroscopy. The observed frequencies of the $[Co_n(N_2)_1]^+$ complexes (n = 8–17) are significantly redshifted (2180 to 2290 cm^{-1}) with respect to the IR inactive vibrations of free N₂ (2359 cm^{-1}). These bands are assigned to a μ_1 head-on type of coordination of the N₂ to the cobalt cluster surface, revealing remarkable cluster size dependent features to interpret.

It is often difficult to investigate heterogeneously catalyzed reactions due to their complexity. Reactions of isolated transition metal clusters may serve to elucidate elementary processes in such reactions. The initial adsorption event is often the rate limiting step in multistep bond activation that precedes any further activation and the phenomenon of gas adsorption in layers became an early subject of research.[1,2] Historically adsorption is classified into chemisorption and physisorption by phenomenological persistence of the adsorbate. Physisorbed species often serve as precursors for activation. The initial adsorption and activation of N₂ is the rate limiting step in the Haber–Bosch process. Therefore the characterization of the precursor state is of great importance for the mechanistic understanding of this catalytic conversion.[3]

CO adsorption on metal surfaces has been characterized by numerous kinetic[4–7] and spectroscopic studies.[8–10] The observed redshift of the CO stretching vibration is understood to indicate the CO coordination site – on top (μ_1), on bridge (μ_2) or on hollow (μ_3). It moreover reflects interaction strength and of course charge effects. Complementary insights arise from the IR based characterization of CO adsorbates on the surfaces of isolated metal clusters.[11–13]

There is equally great interest in the kinetics of the N₂ adsorption on metal surfaces.[14–16] Spectroscopic and kinetic studies of N₂ adsorbed on Fe(111) revealed that there are three

Fachbereich Chemie and Forschungszentrum OPTIMAS,
Technische Universität Kaiserslautern, 67663 Kaiserslautern, Germany

characteristic α-, δ- and γ-states, which refer to side-on, and head-on adsorption to highly and to less coordinated metal surface atoms.[17–19] Many reaction studies have been performed for a better understanding of the N₂ adsorption kinetics with metal clusters.[20–25] Two of these studies[24,25] have drawn far reaching structural conclusions from so called uptake plots of average association numbers of multiple N₂ molecules under flow reactor conditions. They discuss icosahedral, hexagonal (hcp) and face centered cubic (fcc) packing speculating about pressure dependent inter conversion. Despite obvious need merely a single spectroscopic study elucidated the N₂ adsorption on isolated metal clusters, namely those of Ruthenium,[26] with no unambiguous assignment of the recorded spectral features.

Common interpretation of the head-on adsorption of CO and N₂ to surfaces of extended bulk metal samples and of size selected clusters arises in terms of a σ-donor π-acceptor synergistic bonding scheme according to the so called Blyholder model.[27] *Ab initio* DFT modelling reaches its limits when it comes to the appropriate choice of exchange correlation functionals.[7]

The present study probes the N–N stretching frequency of N₂ when adsorbed on size selected cobalt cluster cations at cryogenic temperatures. We aim to gain insight into the binding motifs of the adsorbates and towards the structure of the cobalt clusters themselves. Preliminary *ab initio* DFT calculations augment the current experiments, failing to provide unambiguous structural conclusions as of now.

A customized Fourier Transform-Ion Cyclotron Resonance (FT-ICR)-mass spectrometer (Apex Ultra Bruker Daltonics) served to perform the cluster production, isolation, N₂ condensation, InfraRed Photon Dissociation (IRPD) and mass analysis. The metal clusters were generated using a home-built laser vaporization cluster ion source as described before.[28,29] In brief, cobalt atoms are evaporated from a rotating 1 mm thick cobalt foil by the second harmonic of a pulsed Nd:YAG laser. The hot plasma is captured by a He gas pulse (40 μs, 10–15 bar) created by a home-built piezoelectric valve.[30] The atoms and ions are cooled and aggregate to clusters in the subsequent jet expansion through a 60 mm long channel (2 mm diameter) into vacuum (10^{-6} mbar).

10358 | *Phys. Chem. Chem. Phys.*, 2015, **17**, 10358–10362

This journal is © the Owner Societies 2015

The clusters are skimmed and injected into a cryogenic hexapole ion trap passing different ion lenses, a 90 degrees ion beam bender and a quadrupole mass filter. The ion trap is cooled to 26 K by a closed cycle He cryostat. Buffer or reaction gas can be introduced both pulsed and continuously. In this work we used the continuous gas inlet. He or Ar (He: $[Co_{8-10}(N_2)_1]^+$, Ar: $[Co_{11-17}(N_2)_1]^+$) is used to increase the pressure in the ion trap from 1.7×10^{-7} mbar up to 1.0×10^{-6} mbar to accomplish the efficient trapping and cooling of the ions. The attachment of nitrogen is achieved due to impurities in the buffer gas and can only be observed at temperatures below 28 K. After storage of the ions for a variable time (0–10 s), the manipulated ions are guided by electrostatic lenses into the FT-ICR cell of the so-called "infinity" type.[31] This cell is held at a temperature of 10 K with a closed cycle He cryostat to prevent heating of the clusters by black body radiation. The cell is also used for isolation and detection of the ions.

For the acquisition of the (IRPD) spectra the FT-ICR cell is coupled to a tunable IR laser ($\delta n = 0.9$ cm^{-1}, $\delta t = 7$ ns). This laser is a KTP/KTA optical parametric oscillator/amplifier (OPO/A, LaserVision) system pumped by a pulsed 10 Hz injection seeded Nd:YAG laser (PL8000, Continuum). The difference frequency (DF) between the OPA signal and idler waves is generated in a AgGaSe$_2$ crystal. This generates IR radiation in the range of 1400–2400 cm^{-1}. Each trapped and isolated package of ions is irradiated by 10–15 laser pulses (0.1–1.2 mJ per pulse) to yield a sufficient amount of fragment ions. The IR spectra were recorded as ion chromatograms while continuously scanning the IR wavelength. The IRPD signal was evaluated as $\Sigma_i F_i/(\Sigma_i F_i + \Sigma_i P_i)$, where F_i and P_i indicate fragment and the parent ion signals, respectively. An experimental IRPD spectrum arises from a plot of the fragmentation efficiency as a function of laser frequency. We employed the IRPD spectroscopy in the 2100–2350 cm^{-1} range on the $[Co_n(N_2)_1]^+$ species ($n = 8$–17). In this range we expected the N$_2$ stretching frequencies of the species. For all complexes the loss of the N$_2$ was the only observed fragmentation channel.

The cold IRPD spectra of the cryo cooled $[Co_n(N_2)_1]^+$ cluster adsorbate complexes reveal well resolved bands (cf. Fig. 1). All complexes show a single or multiple IR active bands within the range of 2180 to 2290 cm^{-1} (2110–2350 cm^{-1} probed). These bands are significantly redshifted with respect to the IR inactive stretching mode of free N$_2$ (at 2359 cm^{-1} [32]). Some clusters show multiple bands ($n = 14$–17), other clusters reveal single bands ($n = 8$–13). Dissociative $[N-Co_n-N]^+$ adsorption would inevitably lead to much lower Co–N stretching frequencies which may become as low as 600 cm^{-1} when interstitial nitrides form. Therefore we confirm molecular (intact) adsorption (physisorption) of N$_2$ on naked cobalt cluster surfaces. While we cannot exclude some (at present invisible) dissociation of N$_2$ we do not find forcing evidence. Such an activation would, if any, occur in competition to intact adsorption.

The observed cluster size dependence reveals continuous variations and "jumps"/discontinuities alike. The dotted red line serves to guide the eye. It is slightly tilted towards the red with cluster size. A plain charge dilution effect would lead to an opposite effect namely to a blue shifting by increasing cluster size.
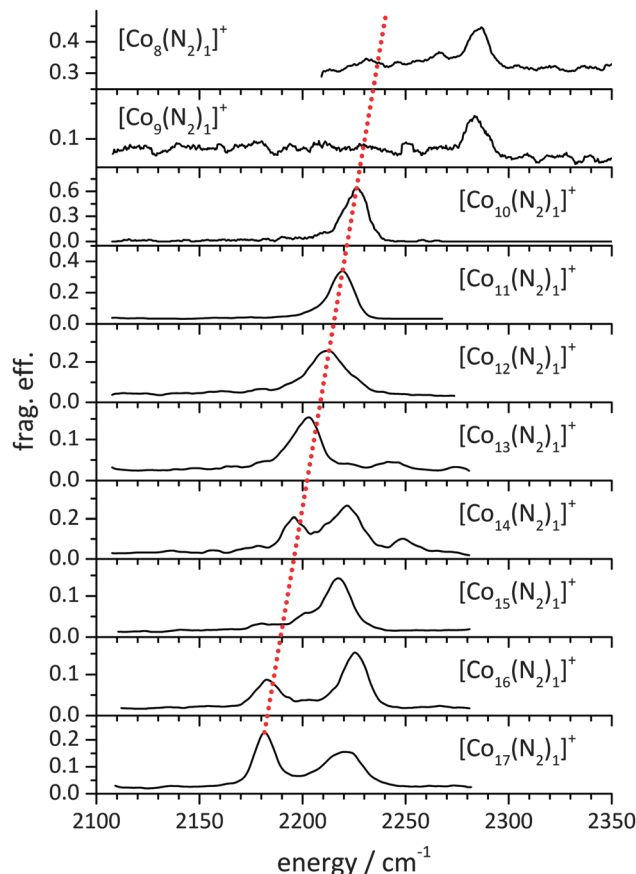

Fig. 1 IRPD spectra of $[Co_n(N_2)_1]^+$ for $n = 8$–17. The dotted red line serves to guide the eye. Its slight tilt with cluster size indicates a conceivable cooperative polarization effect. Note the variation in the observed peak positions and splittings. Multiple major peaks likely indicate cluster core isomers, spin isomers or N$_2$ bonding isomers while weak sidebands to the blue may arise from combination bands (N$_2$ stretching and wagging modes, cf. Table 1). Note the "jump" of the major peak from $n = 9$ to $n = 10$.

Instead one might recall the (likely) metallic nature of the cobalt cluster allowing for electron density shifts in response to external perturbation. Such polarization may couple back to the perturbing adsorbate and enhance electron donation into empty antibinding orbitals – the more the larger the cluster. Hence this would lead to a weakening of the N–N binding strength and an increasing redshift of the stretching frequency with cluster size.

Looking at the bands in detail it is obvious that $[Co_8(N_2)_1]^+$ and $[Co_9(N_2)_1]^+$ do not follow the trend illustrated by the red line. The absorption of $[Co_8(N_2)_1]^+$ and $[Co_9(N_2)_1]^+$ (both at 2285 cm^{-1}) are significantly less redshifted than those of all other cluster complexes studied. The clusters with $n = 10$–13 show merely one strong band that aligns well to the mentioned polarization effect (2226, 2219, 2212, 2203 cm^{-1}). In the case of $[Co_{13}(N_2)_1]^+$ this main absorption band is accompanied by weak sidebands to the blue. These may arise from combination bands (N$_2$ stretching and wagging modes, cf. Table 1, as supported by calculations). Besides these sidebands of $[Co_{13}(N_2)_1]^+$, the main band is in line with a possible icosahedral structure (I_h). A major difference arises

Table 1 Computed vibrations in $[Co_{13}(N_2)_1]^+$ (I_h, $2S + 1 = 15$). Explicitly listed values document all those modes that involve significant motion of either of the two N-atoms

Mode	Type	Freq./ cm^{-1}	Scaled freq./ cm^{-1}	IR intensity/ $km\ mol^{-1}$
ν_1	N_2 wagging	33.8	32.1	0.04
ν_2	N_2 wagging	46.7	44.4	0.08
ν_3	N↑–N–Co↓ bending	78	74	0.17
$\nu_3\cdots\nu_{37}$	Co_{13}^+ skeleton modes	78…306		<2.7
ν_{38}	N↑–N↓–Co↑ bending	354	336	37
ν_{39}	N–N stretching	2338	2221	605

for even larger clusters, which reveal multiple bands. These are possibly due to cobalt cluster isomers, to spin state isomers or to N_2 bonding isomers or to combinations of all three effects. $[Co_{14}(N_2)_1]^+$ is most prominent in revealing three major bands (at 2195, 2222, 2248 cm^{-1}). A possible explanation is the presence of spin isomers. The Co_{14}^+ cluster core structure is conceivable, yet speculative. Our preliminary calculations reveal a possible adatom to a icosahedral core (little overall relaxation), alternatively: significant reorganization (from Co_{13}^+ to Co_{14}^+) through incorporation of the extra Co atom into prior Co_{13}^+ cluster surface, *e.g.* by opening the prior five membered rings to a six membered ring. This would provide for a higher (sixfold) coordinated Co surface atom in the center of the six membered ring. This working hypothesis might serve to explain the new band at 2222 cm^{-1} in $[Co_{14}(N_2)_1]^+$.

A similar picture can be found in $[Co_{15}(N_2)_1]^+$, except for the vanishing "red" peak (which was strong for $[Co_{10-14}(N_2)_1]^+$), indicative of a major change in structural binding motif. Possibly explained by a change from icosahedral to hexagonal close-packed (hcp) as found in larger cobalt clusters by Trapped Ion Electron Diffraction (TIED) experiments (Co bulk: hcp; Co cluster: icosahedral).[33]

DFT calculations of $[Co_{13}(N_2)_1]^+$ (at PBE0/ECP(Co); cc-pVTZ(N) level of theory) reveal full icosahedral I_h geometry of the Co_{13}^+ core with little relaxation by the N_2 attachment. SCF convergence is tedious and can be achieved only by tolerating relaxed SCF convergence criteria of 10^{-5} (as compared to 10^{-8} in "standard" DFT calculations). Choice of an appropriate spin multiplicity is crucial. Our previous XMCD investigations yielded a spin magnetic moment of 2.30(15) μ_B per atom for the Co_{14}^+ cluster.[34] That implies 32(2) unpaired electrons and a multiplicity of $2S + 1 = 33(2)$. Our present DFT calculations have revealed stable high spin state structures of a $[Co_{14}(N_2)_1]^+$ complex with multiplicities 30(+47), 32(0) and 34(+29), relative stabilities in kJ mol^{-1} indicated in parentheses. Both findings are in good agreement – assuming that N_2 adsorption does not alter spin states in Co_{14}^+.

On the basis of this agreement we utilized our DFT approach to undertake an extended search of minimum structures of $[Co_8(N_2)_1]^+$, $[Co_9(N_2)_1]^+$, $[Co_{10}(N_2)_1]^+$ (*cf.* Fig. 3), $[Co_{13}(N_2)_1]^+$, $[Co_{14}(N_2)_1]^+$ and $[Co_{17}(N_2)_1]^+$. The calculations reveal head-on N_2 binding in μ_1 N–Co coordination, irrespective of chosen cobalt cluster geometry – allowing for full relaxation without constraints – and irrespective of chosen N_2 coordination site,

and irrespective of particular spin multiplicity. Other assumed coordinations (μ_2 or μ_3) relax towards μ_1 coordination. This finding is the more important as μ_2 or μ_3 coordinated N_2 would be weak or inactive in the IR. Any activation towards dinitride species was found vastly endothermic. The computed zero Kelvin adsorption enthalpies of N_2 to Co_{13}^+ were found to range around 80 kJ mol^{-1} in case of all likely spin states ($2S + 1 = 25, 27, 29$ and 31), the Co–N distances round 1.890(2) Å. It thus takes two to three IR photons to induce the observed IRPD processes.

Standard *ab initio* calculations reveal force constants and subsequent normal mode analysis reveal harmonic vibrational frequencies. After appropriate lump sum scaling for anharmonicities (empirical factor 0.95) the thus obtained values compare to experimental data. We chose to document the case of $[Co_{13}(N_2)_1]^+$ in more detail (*cf.* Table 1) assuming an icosahedral I_h geometry of Co_{13}^+ (*cf.* Fig. 2). The IR inactive N–N stretching mode of free N_2 at 2359 cm^{-1} redshifts through coordination with Co_{13}^+ to 2203 cm^{-1} (expt.) and 2221 cm^{-1} (calc. ν_{39}) in $[Co_{13}(N_2)_1]^+$. The concomitant N–N–Co bending mode within $[Co_{13}(N_2)_1]^+$ is predicted to occur at 336 cm^{-1} which is outside of our experimental probing range. However, the experimental spectrum reveals weak sidebands to the N_2 stretching mode which locate at $\nu_s(N_2) + 15\ cm^{-1}$, 35 cm^{-1} and (maybe) 68 cm^{-1}. We assign these sidebands to combination modes ($\nu_{39} + \nu_1$), ($\nu_{39} + \nu_2$) and ($\nu_{39} + \nu_3$), which is in qualitative agreement with the DFT computed ν_1, ν_2 and ν_3 values of +32 cm^{-1}, +44 cm^{-1} and +78 cm^{-1}.

Despite all current effort the accordingly computed vibrational spectra of other clusters (as listed above) do not recover the subtle changes in the recorded experimental spectra. Obtained N_2 stretching frequencies do indeed fall into the range of experimental values. There is, however, no further insight from calculations into the origin of the three experimental observations: general and steady increase of N_2 redshift, sudden increase of N_2 redshift when going from $[Co_{8,9}(N_2)_1]^+$ to $[Co_{10}(N_2)_1]^+$, and multiple strong vibrational peaks in the spectra of cluster $[Co_{14}(N_2)_1]^+$ and beyond.

It remains to be seen whether further calculations achieve more insight. Four improvements come to our minds. Broken symmetry
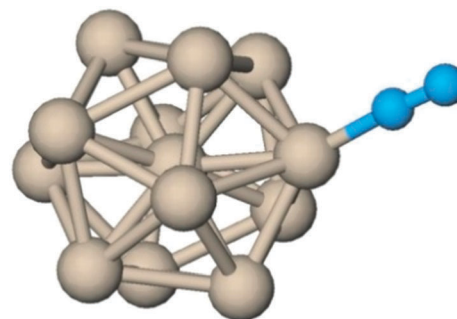
Fig. 2 Computed geometry of $[Co_{13}(N_2)_1]^+$. The assumed icosahedral Co_{13}^+ core is a low lying stable geometry, and it only physisorbs N_2 in μ_1 head-on coordination. Note, that all cobalt surface atoms are equivalent, thus giving rise to a single IR active N–N stretching vibration at about 2230 cm^{-1} (scaled by 0.95) with variations by spin multiplicity of the cobalt cluster core (likely $2S + 1 = 25, 27, 29, 31$) (see text for discussion).
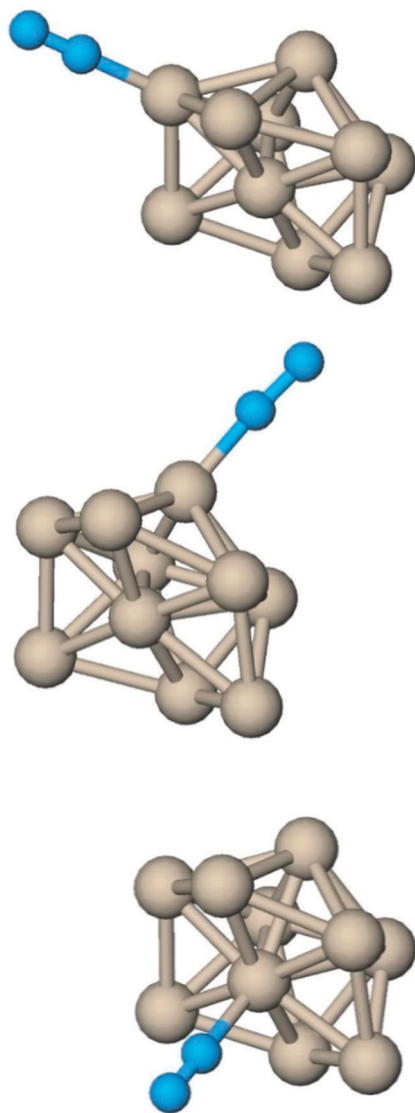
10360 | *Phys. Chem. Chem. Phys.*, 2015, **17**, 10358–10362

This journal is © the Owner Societies 2015

Fig. 3 Three computed geometries of $[Co_{10}(N_2)_1]^+$. The calculated species show the different binding sites of N_2 to the Co_{10}^+ core. N_2 only coordinates μ_1 head-on. The structures differ in the binding motif of the coordination site (Co atom). The structures illustrate an adsorption of N_2 on a Co atom which in turn coordinates to four- (top), five- (middle) or six- (bottom) membered cobalt atom rings. It comes somewhat as a surprise that the present DFT calculations find little variation of N_2 stretching frequencies in response to this change of coordination (e.g. shifts by less than 10 cm^{-1}).

DFT would allow to check for conceivable antiferromagnetic coupling.[35–38] Variation of the DFT functional is mandatory and tedious. Dispersion interaction needs to be considered. Dynamic basin hopping/annealing calculations might retrieve otherwise overlooked geometries.

Conclusions

The N_2 adsorption on cationic Co_n^+ clusters in the size range of n = 8–17 has been investigated via IRPD spectroscopy. The recorded spectra revealed remarkable cluster size dependent features.

All species show bands within the range of 2180 to 2290 cm^{-1}, suggesting a head-on μ_1 coordination of the N_2 on the cluster surface. Current DFT calculations reveal a possible icosahedral Co_{13}^+ core. Nevertheless the calculations do not allow for a final assignment of the observed spectral features (e.g. the "jump" from n = 9 to n = 10 or the presence of multiple bands). It is mandatory to spend further effort in ab initio calculations to gain invaluable insight into the binding motifs of the nitrogen and of conceivable activation routes.

Acknowledgements

Notes and references

1 I. Langmuir, J. Am. Chem. Soc., 1918, **40**, 1361–1403.
2 S. Brunauer, P. H. Emmett and E. Teller, J. Am. Chem. Soc., 1938, **60**, 309–319.
3 G. Ertl, Catal. Rev., 1980, **21**, 201–223.
4 D. M. Cox, K. C. Reichmann, D. J. Trevor and A. Kaldor, J. Chem. Phys., 1988, **88**, 111–119.
5 G. A. Somorjai, Introduction to Surface Chemistry and Catalysis, John Wiley & Sons, 1994.
6 G. Ertl, M. Neumann and K. M. Streit, Surf. Sci., 1977, **64**, 393–410.
7 A. Nilsson and L. G. M. Pettersson, in Chemical Bonding at Surfaces and Interfaces, ed. A. N. G. M. P. K. Nørskov, Elsevier, Amsterdam, 2008, pp. 57–142.
8 A. Crossley and D. A. King, Surf. Sci., 1977, **68**, 528–538.
9 R. M. Hammaker, S. A. Francis and R. P. Eischens, Spectrochim. Acta, 1965, **21**, 1295–1309.
10 F. M. Hoffmann, Surf. Sci. Rep., 1983, **3**, 107–192.
11 A. Fielicke, P. Gruene, G. Meijer and D. M. Rayner, Surf. Sci., 2009, **603**, 1427–1433.
12 A. Fielicke, G. von Helden, G. Meijer, D. B. Pedersen, B. Simard and D. M. Rayner, J. Chem. Phys., 2006, **124**, 194305.
13 J. T. Lyon, P. Gruene, A. Fielicke, G. Meijer and D. M. Rayner, J. Chem. Phys., 2009, **131**, 184706.
14 D. A. King and M. G. Wells, Proc. R. Soc. London, Ser. A, 1974, **339**, 245–269.
15 D. A. King and M. G. Wells, Surf. Sci., 1972, **29**, 454–482.
16 G. Ertl, S. B. Lee and M. Weiss, Surf. Sci., 1982, **114**, 515–526.
17 C. N. R. Rao and G. R. Rao, Surf. Sci. Rep., 1991, **13**, 221–263.
18 M. C. Tsai, U. Ship, I. C. Bassignana, J. Küppers and G. Ertl, Surf. Sci., 1985, **155**, 387–399.
19 J. J. Mortensen, L. B. Hansen, B. Hammer and J. K. Nørskov, J. Catal., 1999, **182**, 479–488.
20 M. B. Knickelbein, Annu. Rev. Phys. Chem., 1999, **50**, 79–115.
21 M. D. Morse, M. E. Geusic, J. R. Heath and R. E. Smalley, J. Chem. Phys., 1985, **83**, 2293–2304.
22 A. Berces, P. A. Hackett, L. Lian, S. A. Mitchell and D. M. Rayner, J. Chem. Phys., 1998, **108**, 5476–5490.

This journal is © the Owner Societies 2015

Phys. Chem. Chem. Phys., 2015, **17**, 10358–10362 | **10361**

23 L. Fuyi, L. Ming, T. Lin and P. B. Armentrout, *J. Chem. Phys.*, 2008, **128**, 194313.

24 J. Ho, E. K. Parks, L. Zhu and S. J. Riley, *Chem. Phys.*, 1995, **201**, 245–261.

25 S. J. Riley, *J. Non-Cryst. Solids*, 1996, **205–207**(Part 2), 781–787.

26 C. Kerpal, D. J. Harding, J. T. Lyon, G. Meijer and A. Fielicke, *J. Phys. Chem. C*, 2013, **117**, 12153–12158.

27 G. Blyholder, *J. Phys. Chem.*, 1964, **68**, 2772–2777.

28 S. Maruyama, L. R. Anderson and R. E. Smalley, *Rev. Sci. Instrum.*, 1990, **61**, 3686–3693.

29 C. Berg, T. Schindler, G. Niednerschatteburg and V. E. Bondybey, *J. Chem. Phys.*, 1995, **102**, 4870–4884.

30 D. Proch and T. Trickl, *Rev. Sci. Instrum.*, 1989, **60**, 713–716.

31 P. Caravatti and M. Allemann, *Org. Mass Spectrom.*, 1991, **26**, 514–518.

32 W. M. Haynes, *CRC Handbook of Chemistry and Physics*, Taylor & Francis, 93rd edn, 2012.

33 T. Rapps, R. Ahlrichs, E. Waldt, M. M. Kappes and D. Schooss, *Angew. Chem., Int. Ed.*, 2013, **52**, 6102–6105.

34 S. Peredkov, M. Neeb, W. Eberhardt, J. Meyer, M. Tombers, H. Kampschulte and G. Niedner-Schatteburg, *Phys. Rev. Lett.*, 2011, **107**, 233401.

35 E. M. V. Kessler, S. Schmitt and C. van Wullen, *J. Chem. Phys.*, 2013, **139**, 184110.

36 C. van Wullen, *J. Phys. Chem. A*, 2009, **113**, 11535–11540.

37 F. Neese, *J. Phys. Chem. Solids*, 2004, **65**, 781–785.

38 F. Neese, *Coord. Chem. Rev.*, 2009, **253**, 526–563.

10362 | *Phys. Chem. Chem. Phys.,* 2015, **17**, 10358–10362

This journal is © the Owner Societies 2015